Chemical Geology 381 (2014) 110–124

Contents lists available at ScienceDirect

Chemical Geology

journal homepage: www.elsevier.com/locate/chemgeo

Weathering on land and transport of chromium to the ocean in a subtropical region (Misiones, NW Argentina): A chromium stable isotope perspective

Robert Frei [a,b,*], Daniel Poiré [c], Karin Margarita Frei [d,e]

[a] Department of Geoscience and Natural Resource Management, Geology Section, University of Copenhagen, Øster Voldgade 10, DK-1350 Copenhagen K, Denmark
[b] Nordic Center for Earth Evolution (NordCEE), University of Copenhagen, Denmark
[c] Centro de Investigaciones Geológicas, Universidad Nacional de La Plata, CONICET, La Plata, Argentina
[d] National Museum of Denmark, Department of Conservation and Natural Sciences, Prinsens Palae, Frederiksholms Kanal 12, DK-1220 Copenhagen K, Denmark
[e] Danish National Research Foundation's Center for Textile Research, SAXO Institute, University of Copenhagen, Karen Blixens Vej 4, DK-2300 Copenhagen S, Denmark

ARTICLE INFO

Article history:
Received 11 February 2014
Received in revised form 30 April 2014
Accepted 2 May 2014
Available online 21 May 2014

Editor: Michael E. Böttcher

Keywords:
Cr isotopes
Weathering profiles
River water
Laterite
Paraná River
Misiones
Argentina

ABSTRACT

We have investigated the pathway of chromium from its mobilization on land and along its riverine transport in a subtropical region of South America (Misiones Province, Argentina), in an attempt to link Cr stable isotope compositions recently measured in seawater with signals prevailing in rivers and, ultimately, with Cr isotope effects observed during oxidative surface weathering in subtropical red soils. Cr concentrations and stable Cr isotopic compositions (expressed as δ^{53}Cr ‰ values) in two typical and representative surface profiles of weathered basalt show significant depletion of Cr in the soils of up to 50%, together with pronounced negatively fractionated δ^{53}Cr values which are indicative of oxidative mobilization of heavy Cr(VI) into the run-off. The behavior of Cr in the studied weathering profiles is not correlated with that of other redox sensitive elements, such as Ce and U; this is essentially due to the affinity of REE and U, but not Cr with secondary phosphates which form during weathering processes.

Smaller tributaries in NW Argentina to the Paraná River (second largest river in South America) carry dissolved Cr in the order of 0.7–1.4 ppb (13–27 nM) with δ^{53}Cr values of +0.2 to +0.4‰, balancing the negatively fractionated weathering products. The isotope composition and concentration of dissolved Cr in the ca. 1200 km long Paraná River from Misiones to its estuary and discharge area into the South Atlantic Ocean remains relatively constant with an average Cr concentration around 2.4 ppb (46 nM) and an average δ^{53}Cr value of +0.32‰. The Cr concentration in the estuary itself drops by ca. 50% but with only minor change in its Cr isotope composition. Results from the Paraná estuary are identical with recently analyzed surface seawater from the Argentine Basin with Cr contents of ~0.3 ppb (~6 nM) and δ^{53}Cr values ~+0.4‰ (Bonnand et al., 2013), and indicate that there is only a minimal Cr isotopic variability during riverine transport, even during long transport distances as shown in our example of the Paraná River. Simple Cr input flux calculations reveal that the Paraná River accounts for ~5% of the total yearly Cr flux to the world's oceans today and that its isotopic signature seems to be, at least locally, imparted to the surface seawater of the Argentine Basin. Whether or not this Cr isotope signature is generally exhibited by the world's oceans needs further investigations, particularly the characterization of seawater around the globe.

1. Introduction

The use of non-traditional isotope systems in the field of geosciences has become an important tool in the understanding and constraining of certain element cycles on Earth, with contributions to geochemical, biochemical and biological aspects therein. The chromium isotope system, in particular, has generated considerable interest and in the last few years there is a growing number of researchers who have developed and employed this system in studies aimed at controlled detoxification/remediation of Cr(VI) contaminated surface- and groundwater (Ellis et al., 2002; Izbicki et al., 2008; Basu and Johnson, 2012; Wanner et al., 2012). In addition, due to the redox sensitivity of the system, it has become a modern tool in attempts to constrain redox conditions in past marine environments (Frei et al., 2009; Frei et al., 2011; Bonnand et al., 2013), and to bridge information to climate driving factors, and thus ultimately to constrain past climate change. In the first instance, chemically precipitated sediments (e.g., iron formations,

* Corresponding author at: Department of Geoscience and Natural Resource Management, Geology Section, University of Copenhagen, Øster Voldgade 10, DK-1350 Copenhagen K, Denmark.
E-mail address: robertf@ign.ku.dk (R. Frei).

http://dx.doi.org/10.1016/j.chemgeo.2014.05.015
0009-2541/

marine carbonates) are potential inventories or archives which could preserve the signature of ancient dissolved Cr species in past seawater. However, before such important links can be used with confidence, it is imperative to understand the release/mobilization mechanisms and pathways of Cr from its potential source regions to the world's oceans, and to understand the mechanisms by which the isotopic signature of Cr can be changed during transport and partitioning into the final geological archive.

A major step forward towards the understanding of the present Cr cycle was achieved by the first measurements of Cr in recent seawater by Bonnand et al. (2013) and by studies investigating the oxidative mobilization of Cr from continental landmasses during present (Berger and Frei, 2013; Crowe et al., in press) and past (Crowe et al., 2013; Frei and Polat, 2013) atmospheric weathering processes. These studies have shown that mobilization through oxidation of trivalent Cr (Cr(III)), made possible by the catalytic help of manganese oxides (Oze et al., 2007), is accompanied by isotopic shifts which render the mobilized Cr(VI) isotopically heavy, and leave behind a weathering product (soil) which is characterized by isotopically light Cr. Oxidation of Cr(III) to soluble hexavalent Cr (Cr(VI)) can therefore enrich the resulting Cr(VI) in the heavy ^{53}Cr isotope by comparison with the residual Cr(III) (Zink et al., 2010). Eventually, the ^{53}Cr-enriched Cr(VI) pool, removed by run-off (Crowe et al., in press), will reach the oceans and render seawater potentially enriched in heavy Cr(VI), as recently confirmed by Bonnand et al. (2013) and our own, unpublished results.

Partial reduction of Cr(VI) in groundwater and/or during riverine transport can potentially further enrich ^{53}Cr in the mobile Cr(VI) pool, whereas light, ^{53}Cr-depleted Cr(III) is immobilized (Ellis et al., 2002, 2004; Jamieson-Hanes et al., 2012; Kitchen et al., 2012; Šillerová et al., 2014). However, the overall effect of Cr redox reactions in the weathering environment leads to heavy Cr(VI) that is ultimately exported to the oceans by rivers where this signal of continental oxidative weathering can be captured by chemical sediments (Frei et al., 2009).

There are essentially two parts of the Cr cycle that need attention: 1) to what degree is the heavy Cr(VI) pool affected by isotopic shift during riverine transport from the site of mobilization to the oceans, and 2) to what degree is the isotopic signature captured in the chemically precipitated archives and does it reflect the isotope composition of dissolved Cr in contemporaneous seawater where these archives form?

In this study we contribute to the understanding of the first of the above-mentioned Cr pathway issues. The study of a modern weathering and transport system in subtropical Argentina is aimed at constraining release mechanisms and associated isotopic changes of Cr during mobilization from basaltic source rocks in an intensive weathering environment into the run-off, as well as the tracing of Cr isotope signals over extensive transport distances in a significant river (Paraná River) and some of its tributaries to the discharge region in the South Atlantic Ocean. Ultimately, we are interested to relate the transported Cr signals to Cr isotope signatures of today's surface seawater in an attempt to create a basis for reconstructing Cr isotope fluctuations of ancient seawater and to create a link to past oxidative weathering processes and thereby a link to climate change on Earth.

2. Regional aspects

The Plata basin is the fourth largest in the world and covers ~20% of the surface of South America (Fig. 1). This hydrographic system extends from the subequatorial zone through the tropics, funneling its numerous tributaries into the Paraná River which discharges into the South Atlantic Ocean and spreads the water along the coasts of Argentina, Uruguay and Brazil (Fig. 1). The Paraná River receives its input through tributaries which to a large degree are dewatering the Paraná Basin, a basin dominated by early Cretaceous basalts of the Paraná Magmatic Province (PMP), one of the largest continental volcanic provinces in the world. The study area where we investigated two representative and typical weathering profiles and collected water samples from several tributaries to the Paraná River is located within the central part (CPMP) of three major magmatic provinces within the PMP. These provinces are separated by the Río Piquiri and Río Uruguay tectonic lineaments (Fig. 1; Piccirillo and Melfi, 1988) and extend from the Iguazú Falls (city of Puerto Iguazú) to the city of Eldorado in the province of Misiones, Argentina. In this part of the PMP, lava flows are predominantly massive to amygdaloidal, with porphyritic varieties, and can be classified as basalts and basaltic andesites (Mena et al., 2006).

The climate in Misiones is controlled by two dominant circulation regimes: (i) the SE trades, which advect moisture to regions near the Atlantic coast (NE Argentina, Uruguay and SE Brazil) and (ii) the South American summer monsoon and the South Atlantic convergence zone, respectively, which result in an austral summer precipitation maximum in tropical and subtropical South America (Vera et al., 2002; Gan et al., 2004). Misiones receives the highest rainfall in Argentina (mean annual precipitation ~1700 mm) except for the southern Cordillera. This is due to the combined influence of high summer and winter precipitation leading to a double rainy season (Prohaska, 1976).

The undulating topography of this region in NE Argentina is the result of a dense network of rivers eroding the basalt formations. The lowest parts of the landscape close to rivers are at an elevation of 150–250 m a.s.l., whereas the upper parts of the plateau are at 550–800 m a.s.l. The resulting topographic gradient between rivers and plateaus is not particularly steep.

3. Samples

3.1. Soil profiles

Two soil profiles were sampled and investigated. One profile (MIS-8) was taken at Minas St. Catalina (25°56′29.35″S, 54°36′34.28″W, Fig. 2). The other profile (MIS-9) is located along Ruta 12 (25°56′18.5″S, 54°34′38.5″W, Fig. 2) near the town of Eldorado. The profiles are depicted in Fig. 3. For each of the profiles, we have collected a least altered basalt either from nearby (in the case of the MIS-9 profile, from an open gravel pit) or from within the base of the profile (in the case of profile MIS-8, a massive, amethyst geode-bearing basalt flow). Similar weathering profiles in the southeastern part of the Paraná Basin within the tropic zone of Brazil have been geochemically classified as laterites Oliveira et al. (1998) and they are petrographically similar to the laterites in other parts of Misiones as described by Zech et al. (1996). The two weathering profiles studied herein can be described in terms of three major sections (Fig. 3a, b):

(i) a recent soil horizon, at its top composed of weathering products of the underlying horizon mixed with plant remains and humic matter. It is darker (medium brown to black) than the underlying horizons and varies in thickness from 5 to about 20 cm.
(ii) a friable, red to reddish brown soil horizon a loose red-clay latosol, which contains dark brown yellow, orange and white glaebules. The interface between this horizon and the lower alterite is irregular and abrupt and at places has a discontinuous stone line which is composed of coarse fragments of lithorelics and alterite debris, embedded in a clayey matrix.
(iii) two alterite facies which occur below the loose red-clay latosol. In profile MIS-8, a boulder facies is composed of large blocks (0.2–0.5 m) with concentric dark orange shells with spongy texture. There are also boulders without cores. The boulder facies grades irregularly downward to a fracture-defined basalt saprock. In profile MIS-9, the latosol horizon passes directly into a saprock, which consists of fragmented, partially mottled rock cut by fissural systems of multidirectional planar pores with white and red clay fillings. The actual contact zone between saprock and fresh basalt is only exposed in profile MIS-8.

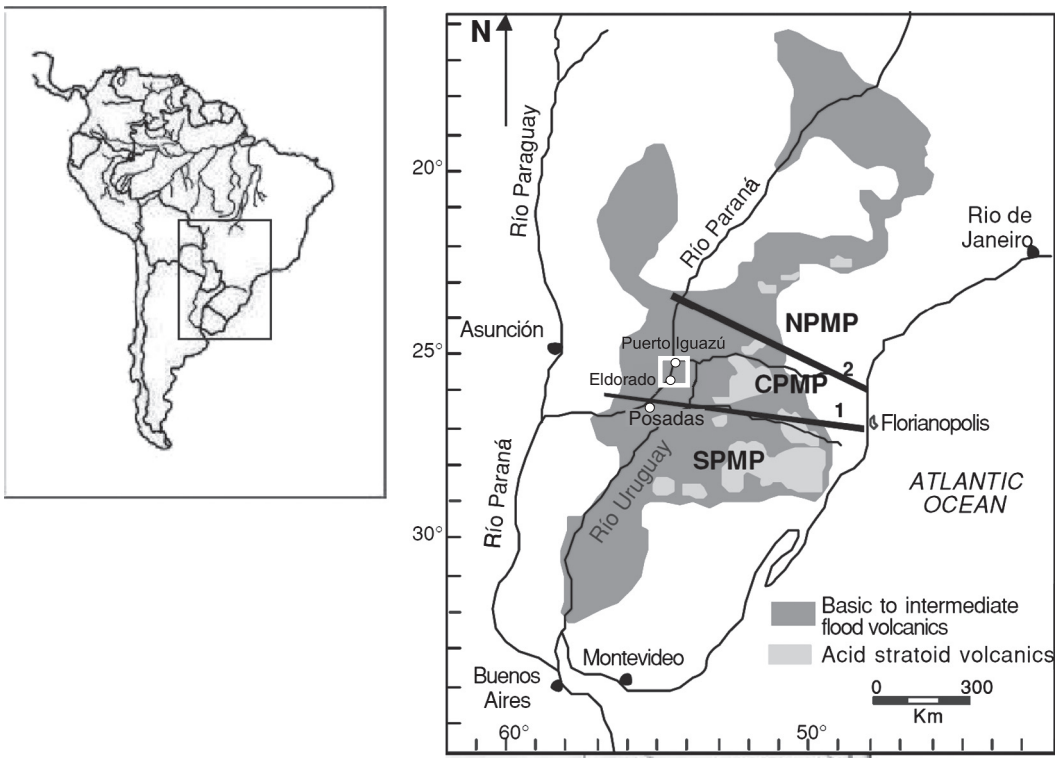

Fig. 1. Sketch map showing the Paraná Magmatic Province (PMP) in South America with its southern-, central and northern sub-provinces, separated from each other by the Río Uruguay (1) and Río Piquiri (2) tectonic lineaments. Modified from Piccirillo and Melfi (1988). The two weathering profiles studied herein and the tributaries sampled are located in the area outlined by the white square within the central (CPMP) part of the PMP, in the NE part of Misiones Province, Argentina.

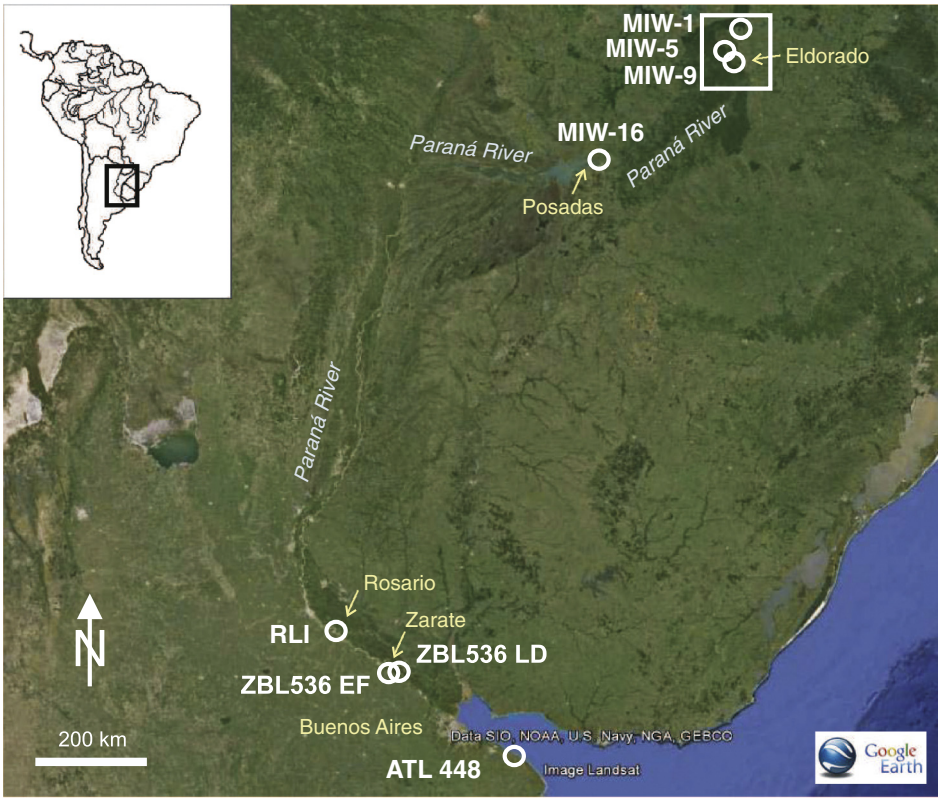

Fig. 2. Google Earth overview map with sample locations of Paraná River samples studied herein. Tributary sample locations and the two studied weathering profiles are within the area outlined by the white rectangle.

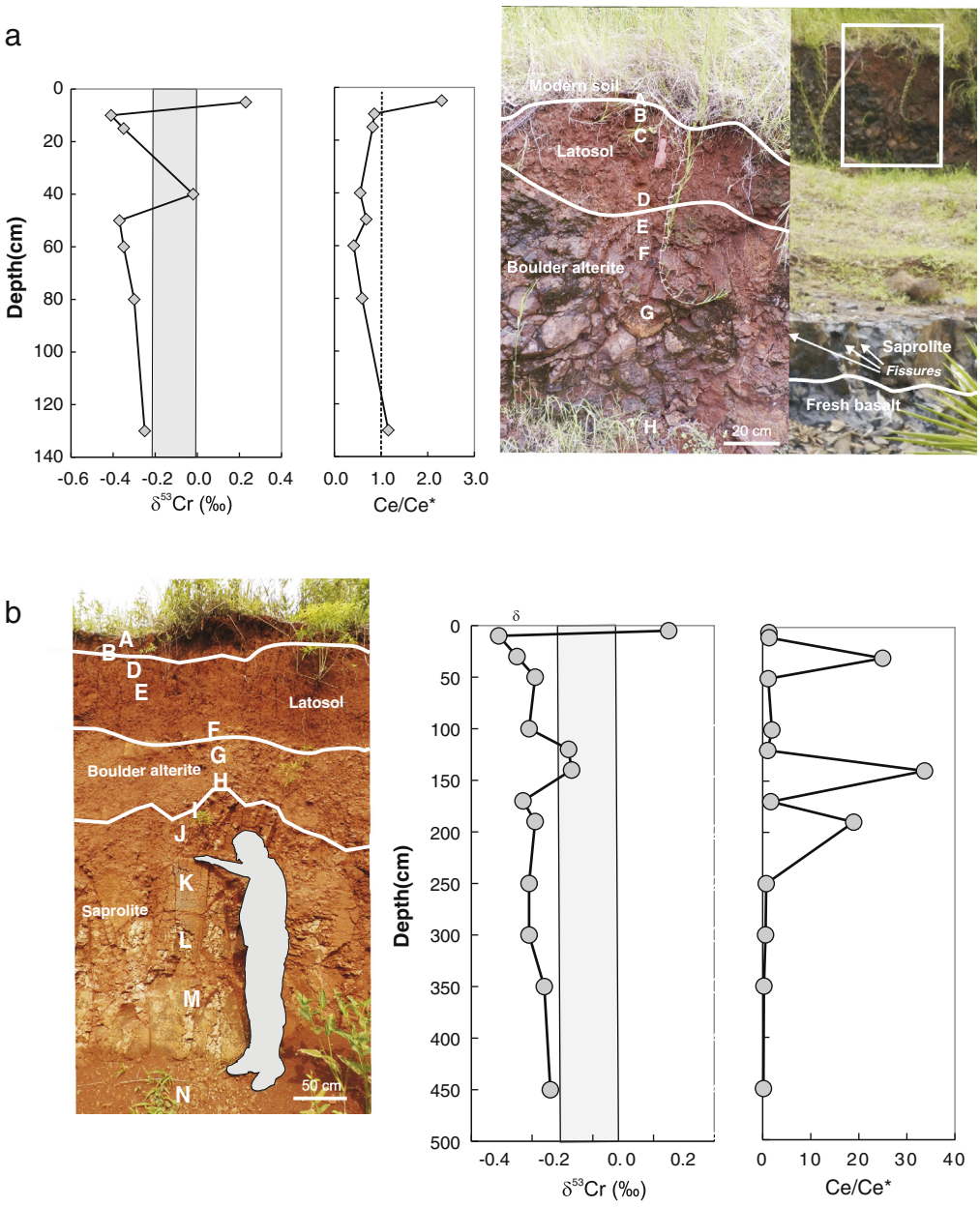

Fig. 3. Field photographs of the two studied weathering profiles MIS-8 (a) and MIS-9 (b), with profile samples indicated at the respective depths. The major subdivisions of the profiles are described in the text. Depth distributions of δ^{53}Cr and Ce/Ce* (Ce anomaly) values (listed in Table 1) accompany the photographs. The gray fields mark the range of δ^{53}Cr values characterizing Earth's high-temperature magmatic inventory (Schoenberg et al., 2008). Errors of δ^{53}Cr values are typically ~0.05‰ (2σ).

3.2. Water samples

Water samples were collected during three successive days in December 2012, in a period dominated by daily thunderstorms. In addition to sampling of major tributaries to the Paraná River in NE Misiones, some smaller creeks were sampled as well. A few water samples from the Paraná River were collected in NE Misiones, one near the city of Posadas, one near Rosario, two near Zarate and one directly in the estuary SE of La Plata (Fig. 2).

4. Methods and analytical details

4.1. Water samples

One liter samples were collected in PP bottles, and passed through 0.2 μm Whatman "Puradisc FP 45 mm" syringe cellulose acetate membrane filters in the field. Measurements of pH were performed simultaneously. We used a Thermo Electron Corporation portable pH meter, type "Orion 3 Star" equipped with a Thermo Orion Scientific, type "Aqua Pro 9103APWP" electrode. Water samples were not acidified and shipped immediately after the fieldwork period, and they were processed in the lab within the first four weeks after sampling in January 2013.

Amounts of 0.5 l of river and creek water were transferred into 0.5 l Erlenmeyer borosilicate glass reaction vessels and spiked with an adequate amount of a ^{50}Cr–^{54}Cr double spike. After evaporation to dryness, 10 ml of concentrated *aqua regia* (Seastar™ high purity concentrated HNO_3 and HCl) was added to the glass reaction vessels and left overnight on a hotplate with an hour glass cover. The acid was then dried again and the sample was dissolved in 50 ml of ultrapure water (MQ system, 18.8 MΩ) and 1 ml of 1 N HCl. Boiling of this solution at 130 °C for half an hour was performed in 100 ml Erlenmeyer borosilicate reaction vessels placed in a sand bath, with

the addition of 1 ml of a saturated ammonium peroxidisulfate ($(NH_4)S_2O_8$) solution to enable oxidation of Cr(III) to Cr(VI). After rapid cooling of the solution, this then was passed over 2 ml anion resin (Biorad™ AG-1X8, 100-200 mesh) charged PP extraction columns. Cr(VI), retained in the resin, was released by reduction to Cr(III) with the help of 10 ml 0.1 N HNO_3 doped with 3 drops of concentrated H_2O_2 into 12 ml Savillex™ Teflon beakers. After drying of this sample on a hotplate at 100 °C, the sample was re-dissolved in 200 μl of 6 N HCl and, with the lid closed, was placed on a hotplate at 100 °C for 2–3 h, during which the beaker was repeatedly tapped to prevent the solution in the beaker evaporating and fully condensing on the beaker's surface. The sample was then diluted with 2 ml ultraclean water and passed over 2 ml of cation exchange resin (AG 50W-8, 100–200 mesh) charged PP columns. The extraction procedure followed a slightly modified recipe of Bonnand et al. (2011) and Trinquier et al. (2008).

4.2. Soil/rock samples

Amounts of ~300 g of soil and rock samples were dried in an oven at 50 °C for 24 h, and then powdered in an agate shatter mill to ensure homogenization. Five gram aliquots were sent to ACME laboratories (Vancouver, Canada), where they were analyzed for major element compositions using ICP-OES (for analytical details, refer to http://acmelab.com/). Fifty milligrams of sample powders were dissolved in 7 ml Savillex™ beakers in a mixture of 2 ml concentrated HF and 3 ml of *aqua regia* (all Seastar™ acids) for 48 h. After drying down the sample solutions, they were taken up with 1 ml concentrated HNO_3 and diluted further to 10 ml with ultrapure water. This solution was analyzed for trace elements using a Perkin Elmer ELAN 6000 DRS ICP-MS at the Geological Survey of Denmark and Greenland (GEUS), using international standards (Govindaraju, 1994). A comparison of GEUS' analytical results on some standards with published values is contained in Kalsbeek and Frei (2006).

An adequate amount of the stock solution prepared for ICP-MS trace element analyses was transferred into a 12 ml Savillex™ Teflon beaker, doped with a ^{50}Cr–^{54}Cr double spike and dried down on a hotplate. The samples were dissolved in 10 ml of 0.1 N HCl to which 3 drops of a 10% ammonium hydroxide solution and 3 drops of concentrated H_2O_2 were added to enable oxidation of Cr(III) to Cr(VI). After about 12 h, the sample solution was then passed over an anion exchange column identical to the one used for the water samples. Subsequently, as with the water samples, the Cr-containing rock/soil sample cuts collected from the anion exchange columns were then further processed over a cation exchange column, using the same elution schemes applied to the water samples. By applying a two column procedure, we obtain highly pure Cr separates. Disturbing anions are efficiently removed from the sample solutions during the oxidation–reduction step in the anion chromatographic separation, whereas cations such as Ca^{2+}, Na^{+}, and Mn^{2+} are removed in the respective cation column elution procedure.

Chromium separates from water and soil/rock samples were measured on an IsotopX, model "Phoenix" TIMS, equipped with eight moveable Faraday collectors, in static mode. Loading and measuring procedures adhere to those reported by Frei and Polat (2013). We report Cr isotope compositions as $\delta^{53}Cr = ((^{53}Cr/^{52}Cr)_{sample} / (^{53}Cr/^{52}Cr)_{SRM\ 979} - 1) \times 1000$, where SRM 979 denotes Standard Reference Material 979. We presently measure and externally reproduce the double spiked SRM 979 Cr standard at $\delta^{53}Cr = 0.08 \pm 0.05‰$ (n = 263), maintaining a ^{52}Cr signal at 5E−12 A (corresponding to a 500 mV beam intensity). The reported $\delta^{53}Cr$ values and respective errors of the samples are calculated as the average of "n" repeated mass spectrometrical runs with their two standard deviations. Procedural Cr blanks were in the order of 4–10 ng and do not affect the measured Cr isotope composition of the waters and soils (with total Cr sample amounts of >350 ng and ≫500 ng) to beyond the external reproducibility of the SRM 979.

5. Results

5.1. Weathering profiles

Soil and rock major and trace elemental data and $\delta^{53}Cr$ values are contained in Table 1. In addition to these values, we also report parameters such as the chemical alteration index (CAI; (Nesbitt and Young, 1982), Ce/Ce* (Ce-anomaly; Lawrence and Kamber, 2006) and La/Yb ratios (indicates the degree of LREE vs. HREE enrichment/depletion), $\sum$REE + Y, and Cr/Al enrichment factors (ER). REE + Y data are plotted in PAAS (post Archean Australian shale; McLennan, 1989) normalized diagrams in Fig. 4.

Both weathering profiles exhibit strong indices of alteration with CAI values ranging between 55 and 99, where fresh basalts display values between 30 and 45 (Nesbitt and Young, 1982; Fedo et al., 1995). The two reference basalts (Basalt; MIS-9) have CAI values of 49 and 51, respectively, and indicate that these basalts are only weakly altered. Profile MIS-9 in particular is strongly weathered as indicated by CAI values >98 throughout the profile sampled (Table 1). These high values are indicative of severe mobilization of the cations Na^{+}, K^{+} and Ca^{2+} relative to immobile Al_2O_3 (Table 1).

REEs, usually considered rather immobile during alteration/weathering processes, offer a means by which to quantify the relative effects of alteration on mobilization of other elements. The exceptions are the two elements Ce and Eu which are redox-sensitive and therefore change their mobility behavior (due to Ce^{3+}–Ce^{4+} and Eu^{3+}–Eu^{2+} transformations) relative to the other REEs. REE + Y patterns of profile samples, compared to respective, least altered reference basalts (Fig. 4) exhibit an overall REE enrichment in the soils (also reflected by the $\sum$REE + Y in Table 1). The shapes of the soil patterns in profile MIS-8 are more or less parallel to those of the reference basalt MIS-6, with significant deviations only in Ce. More variation in the shapes of REE + Y patterns is exhibited by samples from profile MIS-9. Besides huge differences in Ce-anomalies (positive anomalies with Ce/Ce* values up to +33.7 and negative anomalies with Ce/Ce* as low as 0.15; Table 1, Fig. 4b), there is also a significant change in the behavior of LREE. This is expressed in the PAAS normalized La/Yb ratios (La/Yb_{PAAS}), which indicate fractionation between LREE and HREE. In both profiles, LREE depletion relative to HREE is correlated with Ce/Ce* (Fig. 5), in that positive Ce anomalies are more strongly defined in LREE-depleted soils (those with low La/Yb_{PAAS} values).

With respect to Cr, we report Cr enrichment/depletion relative to respective reference basalts as enrichment factors (Cr/Al ER), which compare Cr concentrations relative to Al_2O_3 (considered immobile during weathering, similarly used in assessing the CIA values) of the samples relative to the reference basalts. With the exception of the uppermost, organic rich top soil (sample MIS-8 A) and a sample from 30 cm depth (sample MIS-8 D) in profile MIS-8, which show enrichment of Cr (Cr/Al EF = 2.8 and 1.2, respectively; Table 1), the remaining weathering profile is characterized by significant depletion of Cr of up to 50%. The case is similar in profile MIS-9 where again the organic-rich topsoil (MIS-9 A) and a part between 120 and 140 cm depth (samples MIS-9 G, H) show actual Cr enrichments, whereas the remaining profile samples are characterized by significant Cr depletion (up to 40%). The highest Cr depletion (lowest Cr/Al ER factors) occurs just below the topsoil in both profiles (Table 1).

Stable Cr isotope values (expressed as $\delta^{53}Cr$) of the soils and reference basalts are listed in Table 1 and plotted in Fig. 3 together with the Ce-anomalies. Generally, in both profiles studied, $\delta^{53}Cr$ values are negatively fractionated and exhibit values lower than $\delta^{53}Cr = 0.11 \pm 0.10‰$ defined for terrestrial high-temperature magmatic rocks by Schoenberg et al. (2008). The exceptions to this are the profile samples which show Cr enrichments (positive Cr/Al EF values). These samples exhibit

elevated (in the case of samples MIS-8 A and MIS-9 A even positive) δ^{53}Cr values (Table 1; Fig. 3) up to +0.23‰. The observed signatures, when compared to δ^{53}Cr values of ~−0.13 to −0.15‰ defined by the reference basalts, clearly indicate a redox-dependent mobility of Cr in the weathering profiles. The diagrams in Fig. 6 exhibit a relatively well-defined positive correlation between the degree of depletion/enrichment of Cr and δ^{53}Cr values in both profiles, supporting the fact that Cr mobility is associated with Cr isotopic shifts in such a way that removal of Cr from the profiles leaves behind a soil in which the light isotopes are preferable retained.

5.2. Water samples

Analytical results of water samples are listed in Table 2. Dissolved Cr concentrations vary from 0.7 to 2.8 ppb (13–54 nM; Table 2). Compared to other rivers worldwide (range between 0.1 and 90 ppb (2–1730 nM); Dojlido and Best, 1993) these are on the lower side, although some rivers, such as for example the Yukon River and Columbia River, have also been reported to contain sub-ppb to lower ppb levels of Cr (Cranston and Murray, 1980; Campbell and Yeats, 1984). Isotopically, there is a rather small variation in δ^{53}Cr values in the creek and river waters studied herein. The range of δ^{53}Cr values is from +0.23 to +0.44‰, thus reflecting a positively fractionated (isotopically heavy) total dissolved Cr load throughout the catchment area and downstream along the Paraná River. We notice, however, that the Cr concentrations in the main Paraná River are slightly higher (average of ~2.4 ppb; 46 nM) than those in the different tributaries sampled (average ~1.2 ppb; ~23 nM). Finally, we do not see systematic changes in δ^{53}Cr values downstream along the Paraná River or, on a smaller scale, among the different tributaries in NE Misiones.

6. Discussion

6.1. Chromium in soil/weathering profiles

There is ample evidence from the study of recent and ancient weathering profiles (Berger and Frei, 2013; Crowe et al., 2013; Frei and Polat, 2013; Crowe et al., in press) that ^{53}Cr-enriched Cr(VI) is preferentially lost to run-off leaving the continents with soils containing a ^{53}Cr-poor residue. Acid weathering has previously been proposed as an important source of Cr to the oceans, particularly in association with the rise of oxygen accompanying the Great Oxidation Event (GOE) on Earth (Konhauser et al., 2011). Mobilization of Cr as Cr(III) by acid weathering, promoted by oxidation of pyrite on land, has however been questioned as an important mechanism because of the potential neutralization of locally generated sulfuric acid within the source rocks themselves (Crowe et al., in press). Nonetheless, the isotopic composition of Cr in continental run-off should record the balance between Cr mobilized through oxidation and Cr eventually mobilized through acid dissolution and this, in turn, is expected to control the isotopic composition of seawater (Crowe et al., 2013). Even if Cr(III) mobilization via dissolution was an effective mechanism, it would be unlikely that this mobilization would be accompanied by an isotopic fractionation.

Results presented herein for the two studied laterite profiles indicate that removal of Cr (up to 50%) is associated with isotopic shifts requiring oxidation of Cr(III) to mobile Cr(VI). This is exemplified, with few exceptions (discussed below), by the isotopically light (negatively fractionated δ^{53}Cr values) soils, implying that run-off is isotopically heavy (characterized by positively fractioned δ^{53}Cr values). The entire range of δ^{53}Cr values in the profiles studied is ~0.6‰, less than that observed in the modern Indonesian laterite profile studied by Crowe et al. (in press) where the range of values observed in the soil profile is ~1.5‰, but similar to the range of ~0.8‰ observed in the Paleoproterozoic basaltic paleosols at Schreiber Beach, Ontario, Canada (Frei and Polat, 2013).

Chromium enrichment, coupled with positively fractionated δ^{53}Cr values, occurs in a few defined horizons within both profiles. This has also been observed in other weathering profiles (Berger and Frei, 2013; Crowe et al., 2013; Frei and Polat, 2013; Crowe et al., in press) and clearly demonstrates overprinting by a later process, most likely by the effective and near-complete reductive and adsorptive immobilization of positively fractionated Cr liberated from elsewhere in the profiles.

In both profiles, the uppermost, organic-rich horizon is characterized by high Cr/Al EF and positive δ^{53}Cr ratios (Fig. 6, Table 1). These horizons (see discussion below), are not substantially fractioned with respect to their REE + Y patterns, unlike a few horizons deeper down in the profile with positively fractionated δ^{53}Cr values which exhibit strong positive Ce anomalies and LREE depleted patterns relative to the least altered reference basalts (Fig. 3; Table 1). This renders it likely that it is the higher organic content of these horizons that acts as an effective Cr-trap for surface water run-off. Cr(VI) reduction is an often applied treatment in industrially contaminated sites. Remediation of such contaminated sites commonly consists of Cr(VI) reduction to Cr(III) and/or adsorption. Recently, alternative adsorbents (biosorbents) have been investigated for an effective low-cost treatment of metal-contaminated waters (e.g., Fiol et al., 2008; Šillerová et al., 2014). The study of Šillerová et al. (2014) revealed that the Cr(VI) biosorption process on a few biomaterials was accompanied by heavier Cr isotope enrichment in the remaining Cr(VI) fraction, whereas the sorbed Cr(III) was isotopically light with negative δ^{53}Cr values ranging between −1.2‰ and −2.8‰. If reductive biosorption was responsible for the observed concentrations and isotopic compositions of Cr in the topsoils of the weathering profiles studied herein, then we have to assume that biosorption was an effective and near complete process which would not impart the isotopic shifts towards negatively fractioned δ^{53}Cr values in the sorbed Cr as shown by the study of Šillerová et al. (2014).

Manganese oxides are likely to be responsible for most Cr(III) oxidation in aquatic environments. Fendorf and Zasoski (1992) suggest that $CrOH_2^+$ is the reactive species in this Cr(III) oxidation. Bartlett and James (1979) observed a correlation between the amount of Cr(III) oxidized by soils and the amount of reduced manganese in soils, thereby suggesting that the oxidation of Cr(III) is the result of interaction with manganese dioxides, a process verified by laboratory studies (Palmer and Puls, 1994). Manganese oxides are present in the subsurface as grain coatings, deposits in cracks or fractures, or as finely disseminated grains; sometimes this presence is a result of bacterial activities. The mechanisms for the reaction with MnO_2 occurring at the manganese oxide surfaces (by adsorption of Cr(III) on active surface sites) are complex and not yet fully understood. The Cr(III) oxidation rate is likely related to the amount and surface area of manganese oxides (Schroeder and Lee, 1975; Eary and Rai, 1987), and lab studies indicate this rate to be initially rapid, but subsequently slowing down significantly. Richard and Bourg (1991) explain that the oxidation of Cr(III) by manganese dioxides is likely to occur as a result of several sequential steps, of which the final one involves the desorption of the reaction product species Cr(VI) and Mn(II) and their mobilization into the aqueous phase. Based on the above outlined scenario, one would expect to observe some kind of correlation between Mn and Cr concentrations in the soil profiles, such that Cr depletion would be positively correlated with Mn depletion. This is, however, not shown by our data set (Cr/Al EF vs. Mn/Al EF diagrams not shown here) which might indicate that total Mn concentrations are to a predominant degree controlled by silicate-hosted, lattice bound Mn^{2+}, and not to the MnO_2 coatings directly relevant for the catalytic Cr(III) oxidation.

In their study of a recent laterite profile developed on ultramafic rocks in Indonesia, Crowe et al. (in press) examined the speciation of Cr in the weathering profile using wet chemical extractions and X-ray

Table 1
Major and trace element, and Cr isotope data of weathering profiles.

Element	Unit	MIS-8 A	MIS-8 B	MIS-8 C	MIS-8 D	MIS-8 E	MIS-8 F	MIS-8 G	MIS-8 H
Latitude/longitude		25°56′29.35″S/54°36′34.28″W							
Depth	cm	5	10	15	30	40	50	80	130
SiO_2	%	41.12	37.21	35.96	37.32	40.12	44.13	46.16	46.06
Al_2O_3	%	12.61	17.90	18.59	18.54	17.72	15.07	14.31	12.82
Fe_2O_3	%	25.80	21.51	21.57	21.00	19.73	17.83	16.55	16.89
MgO	%	0.86	1.69	1.87	1.69	1.48	2.20	2.57	3.68
CaO	%	0.42	0.81	0.71	0.63	0.81	3.08	4.84	7.35
Na_2O	%	0.02	0.06	0.01	0.02	0.07	0.94	1.83	2.28
K_2O	%	0.74	0.59	0.49	1.00	1.74	2.23	2.33	0.80
TiO_2	%	5.46	4.94	4.95	5.12	5.00	4.38	4.37	3.93
P_2O_5	%	0.42	0.25	0.27	0.35	0.43	0.64	0.72	0.66
MnO	%	0.33	0.19	0.17	0.23	0.22	0.26	0.23	0.26
Cr_2O_3	%	0.009	0.002	0.003	0.006	0.003	0.003	0.003	0.003
LOI	%	11.8	14.5	15	13.7	12.3	8.8	5.7	4.9
Sum	%	99.76	99.78	99.75	99.75	99.79	99.77	99.78	99.77
TOT/C	%	1.16	0.49	0.49	0.38	0.28	0.14	0.06	0.03
Cr	ppm	62	14	21	38	19	18	20	19
Cr DS	ppm	61.2	14.6	20.0	37.3	19.3	16.6	18.5	18.2
$\delta^{53}Cr$		0.23	−0.41	−0.35	−0.02	−0.37	−0.35	−0.30	−0.25
2σ (n = 4)		0.04	0.06	0.05	0.04	0.04	0.05	0.05	0.03
CIA		91	92	94	92	87	71	61	55
Cr/Al EF		2.8	0.5	0.6	1.2	0.6	0.6	0.7	0.8
Mn/Al EF		1.3	0.5	0.4	0.6	0.6	0.8	0.8	1.0
Ba	ppm	360	548	493	538	601	737	740	634
Ni	ppm	37	45	46	35	32	26	25	22
Sr	ppm	42	76	66	72	70	215	366	513
Zr	ppm	504	453	436	445	423	379	368	334
Sc	ppm	29	38	41	40	38	33	33	30
Sc	ppm	24.74	32.03	31.40	32.50	32.31	19.62	22.48	15.01
V	ppm	584.73	382.40	438.35	452.87	463.82	350.72	367.13	246.98
Co	ppm	40.03	35.17	31.21	38.15	37.92	30.27	32.27	22.17
Ni	ppm	29.91	34.79	32.38	30.94	30.17	20.61	23.56	15.92
Cu	ppm	250.96	335.51	313.26	315.13	306.82	249.61	260.74	138.71
Zn	ppm	146.59	149.90	148.71	144.35	136.28	134.88	135.97	96.89
Ga	ppm	24.08	27.50	29.54	30.31	30.13	24.47	27.49	14.99
Rb	ppm	6.88	7.30	1.44	2.91	6.35	7.78	6.54	2.29
Nb	ppm	40.89	39.82	37.81	38.66	37.12	31.79	33.09	20.41
Cs	ppm	0.19	0.42	0.10	0.17	0.36	0.03	0.02	0.01
La	ppm	35.74	62.84	62.88	68.46	54.59	97.51	102.33	44.50
Ce	ppm	188.67	128.21	141.24	94.48	100.73	94.82	166.17	113.35
Pr	ppm	10.09	17.51	21.37	19.50	18.51	29.49	35.70	12.39
Nd	ppm	42.49	70.57	90.78	76.99	79.26	129.13	154.96	53.36
Sm	ppm	8.98	13.72	18.18	14.87	16.02	25.04	32.03	11.04
Eu	ppm	2.44	3.68	4.90	3.96	4.42	7.32	9.03	3.23
Gd	ppm	8.96	12.50	15.90	12.40	13.47	24.12	28.62	11.18
Tb	ppm	1.41	1.90	2.24	1.77	1.94	3.20	4.10	1.61
Dy	ppm	8.27	11.01	12.04	9.62	10.55	16.43	21.57	8.81
Y	ppm	37.76	45.81	48.72	36.00	35.38	59.14	72.47	36.18
Ho	ppm	1.62	2.09	2.19	1.68	1.84	2.92	3.76	1.68
Er	ppm	4.57	5.96	5.89	4.55	4.91	7.41	9.64	4.38
Tm	ppm	0.68	0.85	0.82	0.62	0.67	0.92	1.25	0.60
Yb	ppm	4.20	5.30	4.80	3.77	3.87	5.02	7.03	3.46
Lu	ppm	0.63	0.75	0.70	0.53	0.55	0.73	0.97	0.51
Hf	ppm	9.15	10.08	9.70	9.73	9.40	8.02	8.69	5.31
Ta	ppm	2.35	2.32	2.21	2.24	2.16	1.84	1.96	1.20
Pb	ppm	11.85	7.90	7.50	7.38	7.67	4.67	4.77	2.97
Th	ppm	2.49	2.77	3.10	4.08	3.39	1.35	1.79	0.59
U	ppm	1.94	1.45	1.27	1.12	1.09	0.82	0.95	0.57
Mo	ppm	1.73	0.95	0.79	0.83	0.86	0.93	0.91	0.82
Ce/Ce*		2.30	0.85	0.82	0.55	0.68	0.41	0.59	1.16
La/Yb_{PAAS}		0.63	0.87	0.97	1.34	1.04	1.43	1.08	0.95
$\sum$REE + Y		357	383	433	349	347	503	650	306

Cr DS = Cr concentration determined by double spike analysis.
Ce/Ce* calculated as $Pr * (Pr / Nd)^2$.
CIA = $M_2O_3/(Al_2O_3 + Na_2O + K_2O + CaO)$.
Cr/Al EF = Cr enrichment factor calculated relative to Al_2O_3 and to the reference basalts.
n = number of repeat mass spectrometric analyses of the same sample load.

spectroscopy. Cr(VI) was present throughout the profile, but the exchangeable fraction, liberated by $CaCl_2$, was generally low in abundance, accounting for about 0.1% of the total Cr in the profile. The more tightly bound Cr(VI) fraction, liberated with phosphate, was present at higher abundance, particularly in the topsoil and in the limonite unit underlying the topsoil where it contributed to 10% of the total Cr. While we have not studied our weathering profiles with respect to Cr speciation, some of the results of Crowe et al. (in press) are conformable with ours. For example, these authors report a shift towards isotopically heavy Cr in the transition zone between the limonite horizon and the underlying

MIS-9 A	MIS-9 B	MIS-9 D	MIS-9 F	MIS-9 G	MIS-9 H	MIS-9 I	MIS-9 J	MIS-9 K	MIS-9 L	MIS-9 M	MIS-9 N	Basalt	MIS-6
25°56′18.5″S/54°34′38.5″W												25°56′14.15″S/ 54°34′36.16″W	25°56′28.79″S/ 54°36′33.76″W
5	10	30	100	120	140	170	190	250	300	350	450		
31.57	35.68	34.88	34.92	34.32	30.95	33.30	32.48	32.66	33.37	37.23	38.92	49.12	48.36
21.03	24.94	25.33	24.96	25.47	24.10	24.99	24.02	22.95	22.16	22.33	20.29	13.14	12.26
25.54	20.46	21.54	22.51	22.16	25.79	23.06	24.98	25.93	25.32	21.53	20.55	14.49	15.26
0.30	0.27	0.28	0.27	0.27	0.20	0.23	0.27	0.30	0.39	0.58	0.92	5.67	4.15
0.23	0.16	0.11	0.09	0.09	0.08	0.10	0.11	0.03	0.04	0.04	0.20	9.93	8.26
0.02	0.01	0.00	0.00	0.01	0.00	0.00	0.00	0.00	0.01	0.01	0.07	2.34	2.66
0.14	0.13	0.11	0.11	0.10	0.10	0.09	0.09	0.06	0.10	0.09	0.25	1.20	0.71
4.62	3.90	4.18	4.30	3.87	4.22	4.25	4.62	4.41	4.19	3.50	3.54	2.34	3.76
0.29	0.17	0.15	0.16	0.24	0.34	0.29	0.31	0.28	0.31	0.36	0.35	0.29	0.61
0.22	0.17	0.15	0.14	0.11	0.20	0.21	0.29	0.19	0.21	0.21	0.22	0.20	0.25
0.065	0.022	0.026	0.032	0.043	0.044	0.029	0.030	0.030	0.028	0.024	0.026	0.019	0.003
15.6	13.8	12.9	12.2	13.0	13.6	13.1	12.4	12.8	13.5	13.7	14.1	0.9	3.3
99.74	99.81	99.78	99.77	99.78	99.73	99.77	99.72	99.74	99.74	99.72	99.65	99.75	99.77
2.32	1.17	0.56	0.30	0.37	0.16	0.16	0.12	0.06	0.07	0.08	0.03	0.02	0.12
445	151	178	219	294	301	198	205	205	192	164	178	130	21.0
447.0	155.0	164.0	204.0	304.0	312.0	211.0	206.0	217.0	189.0	212.0	177.0	128.0	21.1
0.15	−0.41	−0.35	−0.31	−0.18	−0.17	−0.33	−0.29	−0.31	−0.31	−0.26	−0.24	−0.13	−0.15
0.08	0.05	0.07	0.07	0.01	0.02	0.01	0.02	0.02	0.06	0.01	0.02	0.04	0.04
98	99	99	99	99	99	99	99	100	99	99	98	49	51
2.1	0.6	0.7	0.9	1.2	1.3	0.8	0.9	0.9	0.9	0.7	0.9	1.0	1.0
0.7	0.4	0.4	0.4	0.3	0.5	0.6	0.8	0.5	0.6	0.6	0.7	1.0	1.0
131	105	82	94	124	350	291	343	282	261	353	519	309	473
96	95	103	101	91	153	111	122	111	123	102	127	68	30
18	15	13	13	12	12	10	11	6	7	12	33	360	477
371	346	325	355	331	294	303	311	288	279	257	254	157	292
51	48	51	51	58	65	57	60	55	59	67	54	36	29
50.93	46.50	55.37	49.99	56.59	69.00	55.85	59.26	52.72	55.52	65.04	54.23	20.01	12.98
577.25	470.05	417.86	427.90	529.33	578.17	531.28	569.88	579.83	507.02	448.69	485.80	357.87	278.17
57.73	43.99	30.58	32.25	34.11	40.44	52.56	44.30	56.34	82.52	73.33	72.67	39.85	29.15
91.63	86.79	81.65	84.90	86.14	96.68	98.51	90.23	99.73	290.07	163.86	116.58	68.34	21.96
299.81	258.81	212.09	256.26	297.71	280.53	317.73	267.90	307.92	340.43	374.79	413.55	207.30	174.87
148.91	118.55	85.44	106.43	117.62	106.80	120.92	79.63	124.82	272.80	240.65	298.72	96.77	119.63
36.06	34.33	32.01	35.19	36.22	32.88	33.69	31.87	34.07	31.20	30.37	32.34	18.58	20.57
0.49	9.13	0.16	10.12	8.49	0.19	4.47	0.06	2.57	3.70	1.31	1.71	2.96	4.22
33.60	28.17	24.67	30.01	29.96	24.89	27.28	25.78	25.38	23.36	21.87	21.40	15.34	27.06
0.09	3.07	0.12	4.65	3.37	0.05	1.73	0.02	0.72	0.53	0.60	0.10	0.00	0.01
29.94	28.83	28.33	25.39	24.76	4.93	27.76	7.97	42.91	76.16	263.87	579.71	23.49	40.46
94.20	94.54	2380.04	125.80	65.68	519.29	113.12	503.33	73.34	109.30	185.81	207.23	40.82	63.87
8.29	8.14	20.39	7.67	7.28	3.36	7.47	4.80	11.80	22.25	88.81	173.42	6.33	11.12
32.42	32.13	115.92	30.73	29.15	19.26	28.63	25.55	47.36	91.30	376.13	761.12	26.47	46.84
6.78	6.89	53.46	7.09	6.37	9.60	6.15	10.17	9.85	19.29	83.28	166.82	5.10	9.24
1.82	1.90	19.57	1.95	1.71	3.55	1.71	3.47	2.89	5.89	25.18	54.43	1.51	2.62
6.49	6.70	77.89	7.02	6.02	13.85	6.01	12.98	10.02	20.50	81.19	187.53	5.19	8.65
1.01	1.05	17.16	1.17	0.98	3.03	0.98	2.76	1.58	3.19	12.29	28.09	0.72	1.18
5.88	6.26	121.07	7.11	5.91	21.65	5.93	18.69	9.47	18.82	70.04	161.96	4.03	6.22
27.43	29.37	625.48	33.97	26.48	94.80	29.40	66.07	48.75	98.21	302.79	809.46	16.02	20.91
1.16	1.21	27.49	1.43	1.18	4.84	1.21	4.15	1.95	3.84	13.15	30.94	0.79	1.13
3.21	3.43	85.45	4.15	3.44	15.22	3.58	12.44	5.47	10.76	35.31	81.15	2.11	2.93
0.48	0.52	14.56	0.64	0.53	2.67	0.57	2.12	0.83	1.58	4.93	11.07	0.29	0.37
2.91	3.30	96.87	4.21	3.48	17.94	3.80	14.26	5.22	9.94	29.69	64.66	1.69	2.13
0.43	0.50	14.50	0.62	0.51	2.61	0.58	2.15	0.80	1.50	4.29	9.28	0.25	0.30
7.18	6.57	6.06	6.85	7.17	6.49	6.65	6.57	6.56	6.20	6.13	6.32	3.94	6.98
1.81	1.58	1.39	1.68	1.65	1.40	1.42	1.37	1.33	1.25	1.23	1.24	0.79	1.51
19.10	17.31	13.43	16.70	15.23	16.81	13.90	11.96	8.09	7.34	5.86	3.62	2.55	3.61
8.55	7.96	5.80	6.14	7.01	4.10	4.34	3.02	3.67	2.12	0.98	1.06	0.39	0.75
2.50	1.86	1.63	2.02	2.21	2.58	2.02	1.29	1.35	0.78	0.73	0.58	0.49	0.68
2.40	1.87	1.66	1.97	1.96	1.69	1.72	1.61	1.48	11.42	4.29	1.07	0.82	1.15
1.29	1.33	24.96	1.90	1.05	33.67	1.68	18.92	0.72	0.59	0.26	0.15	0.78	0.71
0.76	0.65	0.02	0.44	0.53	0.02	0.54	0.04	0.61	0.57	0.66	0.66	1.03	1.40
222	225	3698	259	183	737	237	691	272	493	1577	3327	135	218

saprock, similar to the shift that we observe in our profile just beneath the limonitic latosol, particularly in profile MIS-9 (Fig. 3, Table 1).

In summary, our results for the two weathering profiles reveal a significant loss (up to 50%) of Cr from the soils, leaving a largely isotopically negatively fractionated (light) alterite behind which is statistically different from the mantle inventory δ^{53}Cr value of -0.1 ± 0.1‰ (Schoenberg et al., 2008), also represented by δ^{53}Cr values of the two least altered basalts in our study. Confirming results from previous studies, our results imply the oxidative removal of isotopically heavy Cr(VI) from subtropical lateritic weathering horizons to the run-off.

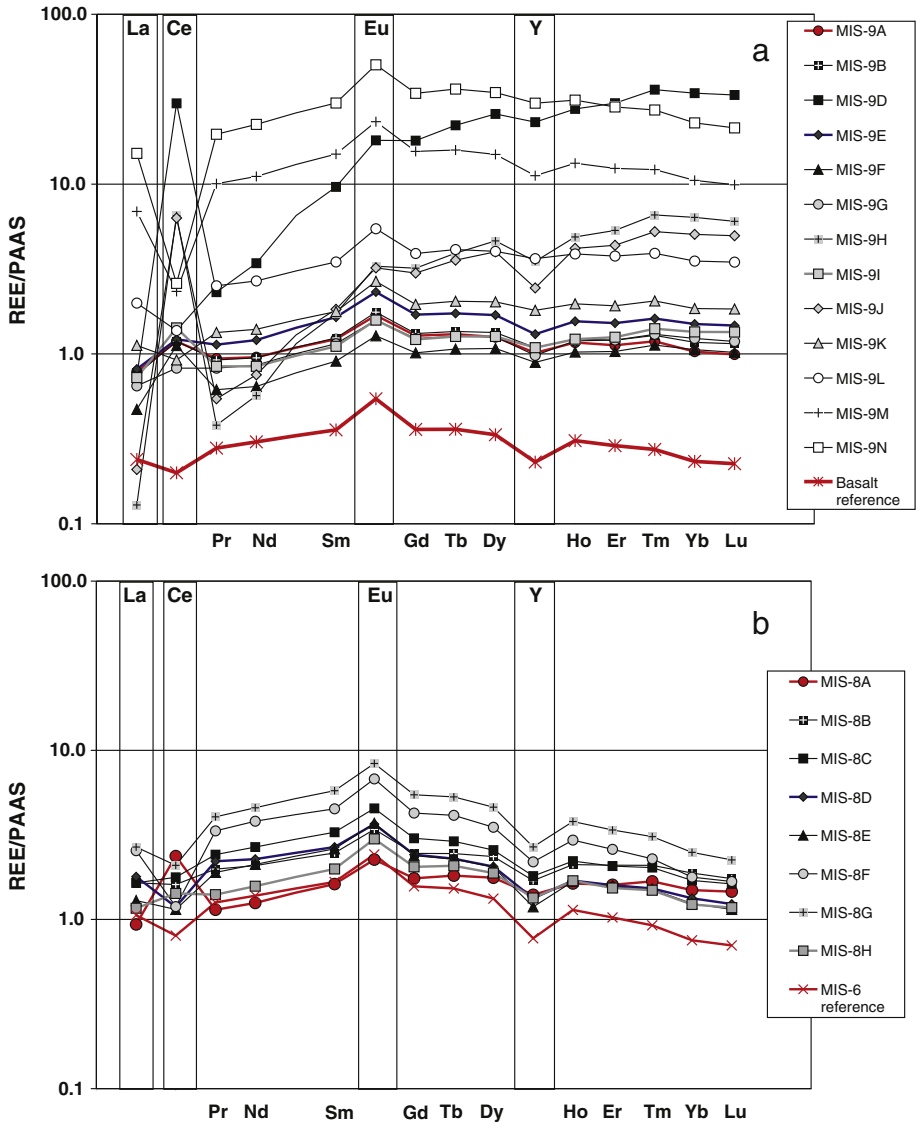

Fig. 4. Post Archean Australian shale (PAAS) normalized REE + Y patterns of samples from profiles MIS-8 (a) and MIS-9 (b). Respective least altered reference basalts and the topsoils of each profile are indicated in red patterns. Variations in the degree of LREE-depletion and magnitude of Ce anomalies are discussed in the text. The apparent enrichment of REE + Y in the weathered samples is due to dilution as a consequence of massive loss of major cations in the weathering basalts during intense weathering (refer to text for details).

6.2. REE + Y in soil/weathering profiles

To study the REE mobility during weathering, it is essential to assess whether the distribution of REEs in the soils is due to the process of chemical weathering, or whether the REEs are inherited from the parent material, in this case the basalts. For example, in profile MIS-8, PAAS normalized REE + Y patterns of the various soil horizons are more or less parallel to those depicted by the least altered reference basalt (sample MIS-6; Fig. 4a). However, on closer inspection, important deviations in the shape of the individual patterns exist, which is for example manifested by differences in the La/Yb ratio and, most pronouncedly, in the Ce/Ce* values (Table 1, Fig. 3). It is difficult to reconcile these patterns with purely magmatic processes, and it is clear that the REE patterns of the soil are to some degree affected by secondary processes that took place after the emplacement of lavas. These secondary processes are even much more visible in profile MIS-9 where huge positive and negative Ce-anomalies are accompanied by variations in LREE depletions, relative to HREE, in the soil horizons. The degree of apparent REE enrichment, more strikingly expressed in profile MIS-9 than in profile MIS-8, is generally reflected by the CAI parameter, which is higher in MIS-9 (98–99) than in MIS-8 (55–94; Table 1). The systematic apparent enrichment of REE + Y in both profiles is interpreted to result from the effect of dilution of whole-rock data, due to the loss of not only major cations such as Ca^{2+}, Na^{+} and K^{+} (components of the CAI parameter), but also Mg (see Table 1) from the weathering basalts. Systematic LREE depletion (expressed by lower La/Yb) in soil horizons of both profiles relative to the reference basalts is compatible with studies showing preferential LREE mobility in low-temperature weathering processes of basalts (Ludden and Thompson, 1979). Secondary phosphates have been postulated as possible hosts of LREE, and their leaching/destruction/re-deposition during interaction with weathering solutions has been proposed as a major control of REE^{3+} mobility (Banfield and Eggleton, 1989; Melfi et al., 1990; Cotten et al., 1995; Berger et al., 2014). Although we have not performed detailed electron microprobe analyses to identify the host phases of the REEs, an indication of the phosphate control on LREE depletion is indicated by a weak negative correlation between P_2O_5 concentrations and La/Yb in both soil profiles, if horizons with strongly positive Ce anomalies are excluded (diagrams not shown). In the latter, cerianite (CeO_2) is likely to control the Ce-distribution in these horizons,

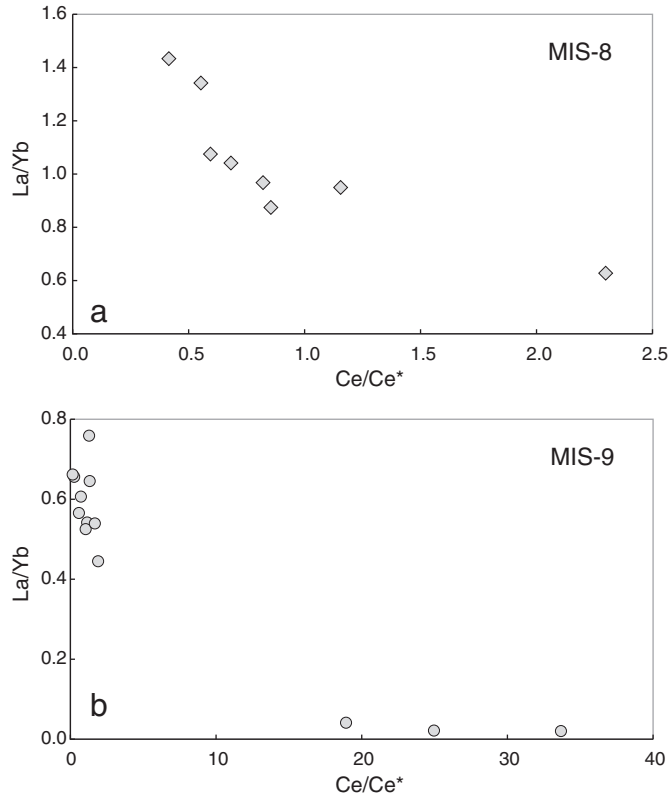

Fig. 5. Diagrams showing the relationships between PAAS-normalized La/Yb values (indicating degree of LREE variations relative to HREE) and Ce-anomalies (expressed as Ce/Ce*) in profiles MIS-8 (a) and MIS-9 (b). With the exception of samples with very positive Ce-anomalies in profile MIS-9, which are attributed to the secondary formation of Ce-oxides in the samples, samples show a weak negative correlation which is interpreted to reflect the control of LREE mobility with secondary phosphates (see text for details).

as shown by a recent study of Berger et al. (2014). U, also a redox sensitive element, correlates in its distributions in the profiles with Ce (except with those samples with very strong positive anomalies which we associate with the occurrence of Ce-oxides (cerianite); respective Ce/Ce* vs. U diagrams not shown herein) and indicates that phosphates play an important control on the redistribution of U in weathering processes.

A prominent feature of the REE + Y pattern in Fig. 4 is the variation in Ce-anomalies, particularly in profile MIS-9. This implies a differential mobilization of Ce relative to the other REEs in the profiles, and is likely to be controlled by redox processes, during which the mobile Ce^{3+} is locally oxidized to Ce^{4+} and therefore immobilized relative to the other REEs transported downward in the weathering profile. Large positive Ce anomalies have been reported in REE-depleted patterns from extremely weathered laterites and bauxites on a range of parent materials (Braun et al., 1990; Boulange and Colin, 1994). Variations in Ce anomalies were also found in spheroidal weathering products of basalts and andesites from Hawaii and Guatemala (Patino et al., 2003). Positive Ce anomalies are here interpreted to derive from precipitation of secondary phosphates and oxides from weathering solutions initially enriched in tetravalent Ce relative to the other trivalent REEs, potentially in localized portions where less altered relicts create the microenvironments with increased pH necessary to immobilize the REEs. We base our interpretation on the observation that soil horizons with strongly positive Ce anomalies are also characterized by the strongest LREE depletion (smallest La/Yb ratios; Table 1). Negative Ce anomalies are considered by us to form as a consequence of preferential mobilization of Ce into the weathering fluids as the oxidized species Ce^{4+}, leaving the soil relatively depleted in Ce compared to the other REEs. Unlike other studies which invoke redistribution of REEs with degree of weathering (Morey and Setterholm, 1997; Braun et al., 1998), our data do not point to systematic changes of REE pattern and Ce anomalies in the weathering profiles with CAI values.

Of special interest in this study was the question whether the redistribution of REEs in the weathering profiles can be correlated with that of Cr. In this regard, the characterization of relationships between Ce and Cr, and Cr isotopes, are of prime importance since both elements are redox-sensitive and thus have the potential to provide information regarding their oxidative mobilization in the aqueous phase. As Fig. 7 shows, there is no correlation between Ce/Ce* values and δ^{53}Cr values in the samples. In profile MIS-9, this can be seen clearly since the soil horizons with strongly positive Ce anomalies (for example samples MIS-9 D and MIS-9 H with Ce/Ce* values of ~33 and ~25, respectively) do not show positively fractionated δ^{53}Cr values. This indicates to us that the redistribution mechanisms and secondary mineral control of Ce and Cr are drastically different and that local conditions in the weathering soils which enable reductive Ce re-precipitation do not have the same effect on reductive Cr immobilization. The exception to this is again the topsoils where we observe the occurrence of small positive Ce anomalies that correspond with both Cr enrichment and positively fractionated δ^{53}Cr values, indicative of effective immobilization of Ce(IV) and enrichment of isotopically heavy Cr(VI) in the fluid, potentially by the organic matter present in this level of the two profiles (see above).

6.3. Chromium in the run-off

Themodynamic data indicate that CrO_4^{2-} and $HCrO_4^-$ should be the dominant dissolved species in oxidized water at a pH range of 5–9, while $Cr(OH)_2^+$ and $Cr(OH)^{2+}$ are the species predicted for reduced waters. Anoxic ground waters and the reducing ability of organic matter could aid in adding Cr(III) to natural waters (Elderfield, 1970). The pH of rivers is generally lower than that of the oceans which would favor the stability of Cr(III). Slow oxidation of Cr(III) to Cr(VI) would allow Cr(III) to persist metastably. Early studies (Pankow et al., 1977) reported that between 34 and 65% of the dissolved Cr in river samples was in the Cr(III) oxidation state. These observations appear to contradict with the solubility data for Cr(III) species and the strong adsorption of Cr(III) to particulate loads would speak for a relatively low concentration of dissolved Cr(III) in river water. This is reflected by studies of dissolved chromium in the St. Lawrence estuary and Columbia River (Cranston and Murray, 1980; Campbell and Yeats, 1984) which showed that the overwhelming proportion (~95%) of dissolved Cr was in the form of CrO_4^{2-}. To our knowledge there are yet no data on the Cr isotopic composition of river waters, perhaps with the exception of the isotopic characterization of the local run-off from open-pit Ni mining operations in Central Sulawesi, Indonesia by Crowe et al. (in press). Our study provides the first comprehensive total dissolved Cr isotope data of a major river whose vast catchment area (Paraná Basin) covers ~20% of the surface of South America. The freshwater samples (rivers, creeks) analyzed herein cover a range of 0.7–2.8 ppb (13–54 nM) dissolved Cr; this is a significantly lower range than the total dissolved Cr concentration of ~1000 nM from the La Manka stream directly dewatering the ophiolite terrain on Sulawesi (Crowe et al., in press), but in the same range as that reported for the Po River (~0.5–2.8 ppb or ~10–54 nM; Pettine et al. (1992)) or the St. Lawrence River (0.14–0.80 ppb, or ~2.7–15.4 nM; Campbell and Yeats (1984)). The concentrations in the Paraná River and its tributaries are also elevated in relation to total dissolved Cr concentrations measured in estuaries worldwide (range of ~0.10–0.43 ppb or ~1.9 to 8.3 nM; (Abu-Saba and Flegal, 1995; Campbell and Yeats, 1984; Cranston and Murray, 1980) and seawater (range from ~0.05 to 0.34 ppb or ~0.9 to 6.6 nM; Achterberg and Van den Berg, 1994; Bonnand et al., 2013; Connelly et al., 2006; Cranston and Murray, 1980; Jeandel and Minster, 1984; Sander and Koschinsky, 2000).

The δ^{53}Cr values measured in the tributaries to the Paraná River, in the Paraná River itself, and in the one estuary sample ATL 448 (Table 1) imply the presence of dissolved heavy Cr, likely present as Cr(VI) species.

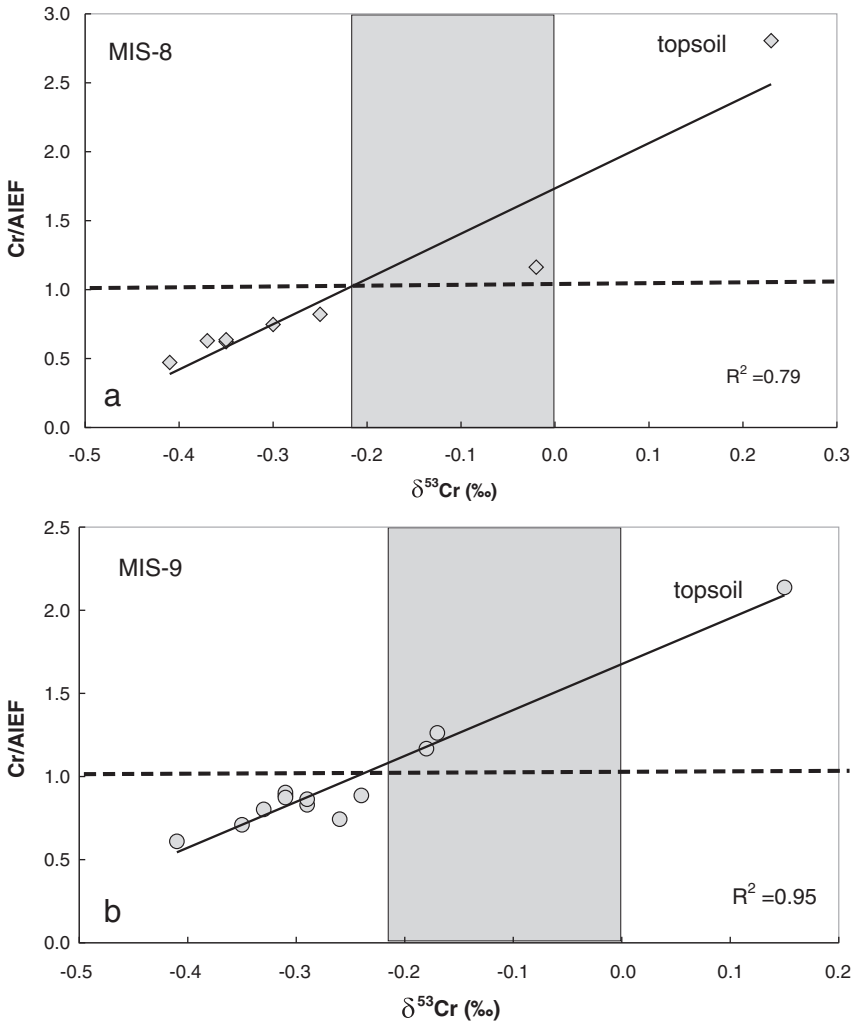

Fig. 6. Diagrams showing the relationship between δ^{53}Cr values and Cr depletion/enrichment, expressed as Cr/Al EF (enrichment/depletion factor EF of Cr relative to immobile Al_2O_3) in profiles MIS-8 (a) and MIS-9 (b). While the majority of samples in both profiles indicate substantial depletion of Cr (low Cr/Al EF values), topsoils and some samples in the transition zone between the latosol and saprock part of the profiles show Cr enrichment which is accompanied by positively fractionated δ^{53}Cr values. The gray field depicts the range of δ^{53}Cr values typical of Earth's high-temperature magmatic inventory as defined by Schoenberg et al. (2008). Errors of δ^{53}Cr values are typically ~0.05‰ (2σ). For discussion refer to text.

Table 2
Cr concentrations, δ^{53}Cr values and pH of water samples from NE Misiones and the Parana River.

	Lat/long		Cr (ppb)	Cr (nM)	δ^{53}Cr (‰)	2σ	n	pH
Sample								
MIW-1	25°35′33.5″S, 54°34′43.6″W	Rio Iguazu, Puerto Iguazu	1.1	21.2	0.36	0.06	2	7.7
MIW-3	25°55′06.6″S, 54°36′34.9″W	Small creek on road to Blomberg	0.8	15.4	0.29	0.07	2	7.4
MIW-4	25°54′56.6″S, 54°36′40.0″W	Arroyo Guatambu	1.4	26.9	0.31	0.05	3	7.6
MIW-5	25°54′59.4″S, 54°37′14.6″W	Rio Parana, Puerto Libertad	2.2	42.3	0.36	0.07	2	7.6
MIW-8	25°56′27.1″S, 54°36′31.2″W	Surface water dripping over pit edge	0.7	13.5	0.23	0.08	2	6.7
MIW-9	26°24′22.8″S, 54°41′40.9″W	Rio Parana, Puerto Eldorado	2.5	48.1	0.44	0.05	3	7.5
MIW-10	26°23′12.1″S, 54°40′53.7″W	Salto Kuipers	1.1	21.2	0.23	0.06	3	7.5
MIW-11	26°23′05.2″S, 54°27′49.5″W	Small creek	1.3	25.0	0.30	0.06	2	7.4
MIW-12	26°21′36.3″S, 54°30′12.6″W	Bridge, Valle Hermoso, Pirai Mini	1.1	21.2	0.42	0.08	2	7.5
MIW-13	26°20′59.6″S, 54°37′02.2″W	Bridge, El Dorado, Pirai Mini	0.9	17.3	0.31	0.06	1	7.6
MIW-14	26°18′03.2″S, 54°37′01.4″W	Bridge, Arroyo Pareha	0.8	15.4	0.45	0.05	2	7.6
MIW-15	26°11′52.2″S, 54°35′13.0″W	Bridge, Arroyo Aguarai Mini	2.8	53.8	0.29	0.06	2	7.7
MIW-16	27°27′46.8″S, 55°48′18.6″W	Rio Parana, near Posadas	2.1	40.4	0.38	0.05	2	7.8
RLI	32°54′58.8″S, 60°39′16.5″W	Rio Parana, Rosario, La Isla	2.5	48.1	0.31	0.06	2	7.7
ZBL536 EF	34°06′18.1″S, 59°0′14.0″W	Rio Parana, Zarate, Brazo Largo Camping E Faro	2.5	48.1	0.41	0.05	3	7.7
ZBL537 LD	33°54′42.6″S, 58°53′22.4″W	Rio Parana, Zarate, Brazo Largo, Campimg La Deolinmda	2.8	53.8	0.40	0.07	2	7.8
ATL 448	35°00′47.4″S, 57°32′8.3″W	Rio Parana, estuary, SW of La Plata	1.1	21.2	0.44	0.06	2	7.9
Averages								
All waters			1.6	31.3	0.35	0.14	(2σ)	
Rio Parana			2.4	46.8	0.38			
Smaller tributaries			1.2	23.1	0.32			

n = number of repeat mass spectrometrical analyses of same sample load.

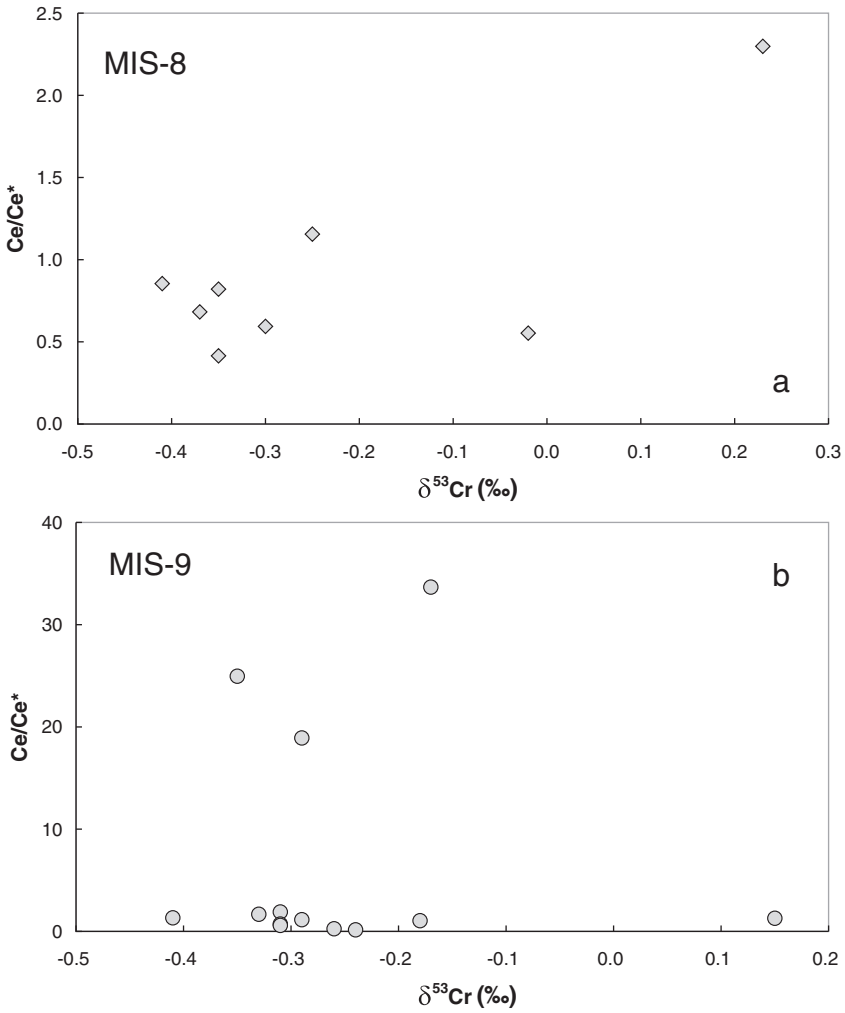

Fig. 7. Diagrams showing the lack of correlation between Ce anomalies (Ce/Ce* values) and δ^{53}Cr values in the weathering profiles MIS-8 (a) and MIS-9 (b). The distribution of LREE, particularly Ce, is advocated to secondary phosphate minerals in the profile which do not have control over the redistribution of Cr. Errors of δ^{53}Cr values are typically ~0.05‰ (2σ).

More recent Cr speciation analyses (combined total Cr and Cr(VI) concentrations) indicate the prevalence of Cr(VI) over Cr(III) in seawater and rivers (e.g., Achterberg and Van den Berg, 1994; Comber and Gardner, 2003; Cranston and Murray, 1980; Isshiki et al., 1989; Mugo and Orians, 1993), which is compatible with our fractioned (isotopically heavy) total dissolved Cr values.

A number of processes can potentially cause back-reduction of dissolved Cr(VI) in the riverine transport and in the estuaries. The major players in the reduction to Cr(III) are dissolved Fe(II), minerals with Fe(II), sulfides (reduced sulfur), and organic matter. The net effect of such reduction would be an isotopic fractionation between the reactant and product, which is characterized by light isotopes in the product (in the reduced Cr(III)) and, conversely, enrichment of the resulting Cr(VI) in the heavy ^{53}Cr isotope. Our study provides the means by which the importance of such reductive processes during riverine transport can be evaluated. Firstly, we do not observe a systematic change of δ^{53}Cr values in the tributary areas and along the ca. 1200 km long Paraná River. The water samples (including the estuary sample ATL 448) define a rather tight average δ^{53}Cr value of $+0.35 \pm 0.14$‰ (2σ, n = 17; Table 1), and the Paraná River sample values do not discriminate from those of the smaller tributaries.

We note, however, that the concentration of dissolved total Cr is about twice as high in the major Paraná River (ca. 2.4 ppb on average) than in the smaller tributaries (ca. 1.2 ppb). The reason for this is unknown, but we suspect that Cr(VI) adsorption as chromate ions may play an important role in the heavy (red-colored) suspend loaded tributaries. Sampling was carried out in a period dominated by thunderstorms and all smaller rivers were loaded with fine reddish soil particles (likely Fe-hydroxides and clays). Ellis et al. (2004) show that sorption of Cr(VI) is not accompanied by isotopic shifts under environmentally relevant pH conditions. Because we do not observe a significant isotopic shift in the total Cr isotope composition of the tributaries, and of the estuary sample, relative to the Paraná River samples we deem Cr(VI) adsorption, rather than its reductive immobilization, a more likely process to explain the lowering of Cr concentrations in these waters. Reductive removal of Cr(VI) would certainly have resulted in excessive δ^{53}Cr variation and certainly would have had the net effect of leaving the remaining dissolved Cr(VI) isotopically even heavier. Our results find support in the study of Cr in the Columbia River by Cranston and Murray (1980) who found dissolved CrO_4^{2-} generally to behave rather conservatively in the estuary. However, some removal of dissolved Cr(VI) was identified in sediments up to 115 km from the river mouth, and these authors explained this to be related to the formation of particles (iron oxide–organic matter colloids) which flocculate when seawater cations neutralize the negatively charged colloids (Boyle et al., 1977).

6.4. The river–seawater connection

In order to make a step forward in putting together the stages for a better understanding of a complex Cr cycle, we need to understand how, if at all, the Cr additions to the ocean are reflected by the Cr isotope compositions of the seawater, and, eventually, whether this signal can be

imparted to materials which form directly as chemical precipitates in the marine environment. The study presented herein contributes to the first question on how a riverine Cr isotope signal compares to that of contemporaneous seawater into which the river discharges its dissolved loads. Our study reveals that the total dissolved Cr isotope signature of the tributaries and the Paraná River yields a rather well defined average of $\delta^{53}Cr = +0.34 \pm 0.14‰$ (2σ; n = 17), implying conservative behavior of Cr during transport. Although we have not characterized the surface waters with respect to speciation of Cr, based on the above discussion and existing Cr data bases of rivers and estuaries, we argue for predominance of Cr(VI) over Cr(III) during the entire riverine pathway of Cr in NE Argentina from its mobilization from the lateritic soils to the discharge area. Our results strongly support those of Cranston and Murray (1980) with respect to Cr(VI) in the Columbia River and estuary.

A recent study by Bonnand et al. (2013) reports, for the first time, $\delta^{53}Cr$ for seawater from open ocean. They publish total dissolved Cr concentrations and Cr isotope compositions of a water column in the Argentine Basin, a location which is situated off-shore, to the south of the Paraná discharge area in the South Atlantic Ocean. We can therefore directly compare the discharge area signals and the riverine Cr isotope signal with these offshore values. The average $\delta^{53}Cr$ value determined herein for the transported dissolved Cr of $+0.34 \pm 0.14‰$ lies statistically within the range of $\delta^{53}Cr$ values between +0.41 and +0.56‰ for the seawater of the Argentine Basin (Bonnand et al., 2013). In particular, our value measured in the estuary (sample ATL 448) with a $\delta^{53}Cr$ value of $+0.44 \pm 0.06‰$ compares well with the Argentine Basin water at 30 m depth (surface water) with a $\delta^{53}Cr$ value of $+0.41 \pm 0.04‰$ reported by these authors. While the drawing of hard-and-fast conclusions is not possible at this stage (more detailed investigations have to be undertaken in the future to constrain them), we tentatively propose that a total dissolved Cr isotope signal carried by a major and significant river like the Paraná River studied herein is reflected by the local ocean surface water signal. With respect to total dissolved Cr concentrations, our study, when compared to that of Bonnand et al. (2013), reveals that lowering of the concentration in the Paraná River (average of 2.4 ppb; 46 nM) to ~1.1 ppb (21 nM) in the estuary and to ~0.3 ppb (6 nM) in the open ocean (Bonnand et al., 2013) is probably either due to dilution of the river water by seawater only and/or due to removal of Cr(VI) by simple adsorption onto or flocculation with freshly formed particles as proposed by Cranston and Murray (1980).

6.5. Paraná River Cr flux to the South Atlantic Ocean

The data set provided herein allows us to constrain the total dissolved Cr flux of the Paraná River into the South Atlantic and to estimate its proportion relative to the total riverine input into the world's oceans. If we take our average total dissolved Cr concentration of 2.4 ppb (46 nM) for the Paraná River as the input value, and use the discharge value of 22,000 $m^3\ s^{-1}$ reported by Piola et al. (2005) for the Paraná River into the South Atlantic, then we calculate a total yearly Cr input of the Paraná River system into the oceans of $3.12 * 10^7$ mol y^{-1}. Compared to the total riverine Cr influx to the world's oceans of $6.3 * 10^8$ mol y^{-1} proposed by Elderfield and Schultz (1996), we then calculate that the Paraná River influx contributes about 5% to that flux. This is a remarkably high contribution, and is based on the relatively high total dissolved Cr concentrations measured in the Paraná River, relative to a range of 0.05–0.9 ppb (1–17 nM) value used by Bonnand et al. (2013) in their Cr flux modeling. We consider two reasons for this elevated riverine Cr flux: 1) Since we have collected the water samples during a period in the rainy season in December when weathering is expected to be enhanced by daily thunderstorms, it is likely that the Cr concentrations measured in the river waters are not representative for depicting yearly averages, but rather could be seen as maximum values. Consequently, the calculated Cr flux to the oceans by the Paraná River using the 46 nM average would then be a maximum flux. 2) The catchment area of the Paraná River is dominated by basalts of the Paraná Magmatic Province with relatively high concentrations of Cr. Weathering of these basalts could favorably lead to release and mobilization of larger fractions of Cr into the rivers. Since we consider both of the above reasons likely to contribute to the elevated concentration of dissolved Cr in the analyzed water samples, we conclude that, the Paraná River is an exceptionally important river when considering the input flux of Cr into the modern oceans, and it may have a significant impact on the modern isotope composition of ocean water, at least of the South Atlantic Ocean.

7. Conclusions

Our study provides ample evidence for positively fractionated (isotopically heavy) Cr in river water that is discharged by the Paraná River into the South Atlantic Ocean, a scenario that was recently proposed by Bonnand et al. (2013) which they based on mass balance modeling to explain positively fractionated $\delta^{53}Cr$ values measured by them in ocean water. Our results indicate that $\delta^{53}Cr$ values average a value of $+0.34 \pm 0.14‰$ and do not significantly change in the catchment tributaries and the main Paraná River over transport distances of more than 1200 km, from areas dominated by intense sub-tropical weathering of basalts in NE Argentina to the discharge area.

Compared to recent Cr isotope analyses of South Atlantic ocean waters by Bonnand et al. (2013), we conclude that the Paraná River signal is imparted to ocean water, and that the Paraná River contributes ~5% to the total dissolved Cr flux in the world's oceans today.

We also provide evidence, and support earlier results of our group, that Cr isotopes are fractionated during sub-tropical weathering, enriching the run-off with heavy Cr(VI), and leaving the alterite with a light Cr isotope signature. Our data indicate that under the weathering conditions prevalent in NE Argentina today, up to 50% of Cr originally contained in the basalts pertaining to the Paraná Magmatic Province is removed from the soils.

Our detailed major and trace element study of two weathering profiles in the province of Misiones indicates Cr enrichment up to 280% in the topsoils which we explain by effective and rapid reduction of mobilized Cr(VI) to Cr(III) by organic matter. Comparison of Cr release/redistribution in the weathering profiles with other redox sensitive elements (Ce, U) reveals that Cr mobility is not correlated with the distribution patterns defined by the latter. Variations in the magnitude of positive and negative Ce anomalies, and LREE depletion relative to HREE in the profiles, are possibly due to the formation of secondary LREE rich phosphates, the formation of which has no effect on the redistribution/re-deposition of Cr within the clay-dominated latosols in the upper part of the profiles. Redistribution at depth of Cr in both profiles is attributed to reductive immobilization of Cr(VI)-containing waters in parts of the profile where relict Fe^{2+}-bearing mineral phases are fragmentally preserved.

At this stage, in order to better understand the Cr cycle, it is imperative to investigate other river catchment systems (also in colder climatic regions) and to characterize the behavior of dissolved Cr loads in the entire transport pathway to the respective estuaries, where the transported signals can be compared to $\delta^{53}Cr$ values of modern seawater from around the globe, an investigation which we hope to contribute to in the near future.

Acknowledgments

We are thankful for the help of Toni Larsen with ion chromatographic separations and thank Toby Leeper for always maintaining the mass spectrometers in perfect running conditions. John Bailey has provided an internal review, and we acknowledge his valuable input. Financial support through the Danish Agency for Science, Technology and Innovation grant nr. 11-103378 to RF and through the Danish National Research Foundation's centers of excellence NordCEE (DNRF grant number DNRF53) and CTR (DNRF grant number DNRF64) is highly appreciated. We are grateful to the constructive comments of two anonymous reviewers which greatly improved our initial manuscript.

References

Abu-Saba, K.E., Flegal, A.R., 1995. Chromium in San Francisco Bay: superposition of geochemical processes causes complex spatial distributions of redox species. Mar. Chem. 49, 189–199.

Achterberg, E.P., Van den Berg, C.M.G., 1994. Automated voltammetric system for shipboard determination of metal speciation in sea water. Anal. Chim. Acta. 284, 463–471.

Banfield, J.F., Eggleton, R.A., 1989. Apatite replacement and rare earth mobilization, fractionation, and fixation during weathering. Clay Clay Miner. 37, 113–127.

Bartlett, R.J., James, B., 1979. Behavior of chromium in soils: III: oxidation. J. Environ. Qual. 8, 31–35.

Basu, A., Johnson, T.M., 2012. Determination of hexavalent chromium reduction using Cr stable isotopes: isotopic fractionation factors for permeable reactive barrier materials. Environ. Sci. Technol. 46, 5353–5360.

Berger, A., Frei, R., 2013. The fate of chromium during tropical weathering: a laterite profile from Central Madagascar. Geoderma 213, 521–532.

Berger, A., Janots, E., Gnos, E., Frei, R., Bernier, F., 2014. Rare earth element mineralogy and geochemistry in a laterite profile from Madagascar. Appl. Geochem. 41, 218–228.

Bonnand, P., Parkinson, I.J., James, R.H., Karjalainen, A.-M., Fehr, M.A., 2011. Accurate and precise determination fo stable Cr isotope compositions in carbonates by double spike MC-ICP-MS. J. Anal. At. Spectrom. http://dx.doi.org/10.1039/c0ja00167h.

Bonnand, P., James, R.H., Parkinson, I.J., Connelly, D.P., Fairchild, I.J., 2013. The chromium isotopic composition of seawater and marine carbonates. Earth Planet. Sci. Lett. 382, 10–20.

Boulange, B., Colin, F., 1994. Rare earth mobility during conversion of nepheline syenite into lateritic bauxite at Passo Quatro, Minais Gerais, Brazil. Appl. Geochem. 9, 701–711.

Boyle, E.A., Edmond, J.M., Sholkovitz, E.R., 1977. The mechanism of iron removal in estuaries. Geochim. Cosmochim. Acta 41, 1313–1324.

Braun, J.J., Pagel, M., Muller, J.-P., Bilong, P., Michard, A., Guillet, B., 1990. Cerium anomalies in lateritic profiles. Geochim. Cosmochim. Acta 54, 781–795.

Braun, J.J., Viers, J., Dupre, B., Polve, M., Ndam, J., Muller, J.P., 1998. Solid/liquid REE fractionation in the lateritic system of Goyoum, East Cameroon: the implication for the present dynamics of the soil covers of the humid tropical regions. Geochim. Cosmochim. Acta 62, 273–299.

Campbell, J.A., Yeats, P.A., 1984. Dissolved chromium in the St. Lawrence estuary. Estuar. Coast. Shelf Sci. 19, 513–522.

Comber, S., Gardner, M., 2003. Chromium redox speciation in natural waters. J. Environ. Monit. 5, 410–413.

Connelly, D.P., Statham, P.J., Knap, A.H., 2006. Seasonal changes in speciation of dissolved chromium in the surface Sargasso Sea. Deep-Sea Res. I 53, 1975–1988.

Cotten, J., Le Dez, A., Bau, M., Caroff, M., Maury, R.C., Dulinski, P., Fourcade, S., Bohn, M., Brousse, R., 1995. Origin of anomalous rare-earth element and yttrium enrichments in subaerially exposed basalts: evidence from French Polynesia. Chem. Geol. 119, 115–138.

Cranston, R.E., Murray, J.W., 1980. Chromium species in the Columbia River and estuary. Limnol. Oceanogr. 25, 1104–1112.

Crowe, S.A., Døssing, L.N., Beukes, N.J., Bau, M., Kruger, S.J., Frei, R., Canfield, D.E., 2013. Atmospheric oxygenation three billion years ago. Nature 501, 535–539.

Crowe, S.A., Døssing, L.N., MacLean, L.C.W., Nomosatryo, S., Fowle, D.A., Mucci, A., Frei, R., Canfield, D.E., 2014. Oxidative weathering fractionates Cr isotopes. Earth Planet. Sci. Lett. (in press).

Dojlido, J.R., Best, G.A., 1993. Chemistry of Water and Water Pollution. Ellis Horwood Limited, New York,.

Eary, L.E., Rai, D., 1987. Kinetics of chromium(III) oxidation to chromium(VI) by reaction with manganese-dioxide. Environ. Sci. Technol. 21, 1187–1193.

Elderfield, H., 1970. Chromium speciation in sea water. Earth Planet. Sci. Lett. 9, 10–16.

Elderfield, H., Schultz, A., 1996. Mid-ocean ridge hydrothermal fluxes and the chemical composition of the ocean. Annu. Rev. Earth Planet. Sci. 24, 191–224.

Ellis, A.S., Johnson, T.M., Bullen, T.D., 2002. Chromium isotopes and the fate of hexavalent chromium in the environment. Science 295, 2060–2062.

Ellis, A.S., Johnson, T.M., Bullen, T.D., 2004. Using chromium stable isotope ratios to quantify Cr(VI) reduction: lack of sorption effects. Environ. Sci. Technol. 38, 3604–3607.

Fedo, C.M., Nesbitt, H.W., Young, G.M., 1995. Unraveling the effects of potassium metasomatism in sedimentary rocks and paleosols, with implications for paleoweathering conditions and provenance. Geology 23, 921–924.

Fendorf, S.E., Zasoski, R.J., 1992. Chromium(III) oxidation by δ-MnO_2. 1. Characterization. Environ. Sci. Technol. 26, 79–85.

Fiol, N., Escuerdo, C., Villaescusa, I., 2008. Chromium sorption and Cr(VI) reduction to Cr(III) by grape stalks and yohimbe bark. Bioresour. Technol. 141, 145–151.

Frei, R., Polat, A., 2013. Chromium isotope fractionation during oxidative weathering — implications from the study of a Paleoproterozoic (ca. 1.9 Ga) paleosol, Schreiber Beach, Ontario, Canada. Precambrian Res. 224, 434–453.

Frei, R., Gaucher, C., Poulton, S.W., Canfield, D.E., 2009. Fluctuations in Precambrian atmospheric oxygenation recorded by chromium isotopes. Nature 461, 250–253.

Frei, R., Gaucher, C., Døssing, L.N., Sial, A.N., 2011. Chromium isotopes in carbonates — a tracer for climate change and for reconstructing the redox state of ancient seawater. Earth Planet. Sci. Lett. 236, 28–40.

Gan, M.A., Kousky, V.E., Ropelewski, C.F., 2004. The South American monsoon circulation and its relationship to rainfall over West-Central Brazil. J. Clim. 17, 47–66.

Govindaraju, K., 1994. 1994 compilation of working values and sample description for 383 geostandards. Geostand. Newslett. 18, 1–158.

Isshiki, K., Sohrin, Y., Karatani, H., Nakayama, E., 1989. Preconcentration of chromium(III) and chromium(VI) in sea-water by complexation with quinolin-8-ol and adsorption on macroporous resin. Anal. Chim. Acta. 224, 55–64.

Izbicki, J.A., Ball, J.W., Bullen, T.D., Sutley, S.J., 2008. Chromium, chromium isotopes and selected trace elements, western Mojave Desert, USA. Appl. Geochem. 23, 1325–1352.

Jamieson-Hanes, J.H., Amos, R.T., Blowes, D.W., 2012. Reactive transport modeling of chromium isotope fractionation during Cr(VI) reduction. Environ. Sci. Technol. 46, 13311–13316.

Jeandel, C., Minster, J.F., 1984. Isotope-dilution measurement of inorganic chromium(III) and total chromium in seawater. Mar. Chem. 14, 347–364.

Kalsbeek, F., Frei, R., 2006. The Mesoproterozoic Midsommerso dolerites and associated high-silica intrusions, North Greenland: crustal melting, contamination and hydrothermal alteration. Contrib. Mineral. Petrol. 152, 89–110.

Kitchen, J.W., Johnson, T.M., Bullen, T.D., Zhu, J., Raddatz, A., 2012. Chromium isotope fractionation factors for reduction of Cr(VI) by aqueous Fe(II) and organic molecules. Geochim. Cosmochim. Acta 89, 190–201.

Konhauser, K.O., Lalonde, S.V., Planavsky, N.J., Pecoits, E., Lyons, T.W., Mojzsis, S.J., Rouxel, O.J., Barley, M.E., Rosiere, C., Fralick, P.W., Kump, L.R., Bekker, A., 2011. Aerobic bacterial pyrite oxidation and acid rock drainage during the Great Oxidation Event. Nature 478, 369–373.

Lawrence, M.G., Kamber, B.S., 2006. The behaviour of the rare earth elements during estuarine mixing-revisited. Mar. Chem. 100, 147–161.

Ludden, J.N., Thompson, G., 1979. An evaluation of the behavior of the rare earth elements during the weathering of sea-floor basalt. Earth Planet. Sci. Lett. 43, 85–92.

McLennan, S.M., 1989. Rare earth elements in sedimentary rocks: influence of provenance and sedimentary processes. Rev. Mineral. Geochem. 21, 169–200.

Melfi, A.J., Figueiredo, A.M., Kronberg, B.I., Dohert, W.D., Marques, L.S., 1990. REE mobilities during incipient weathering of volcanic rocks of the Parana Basin, Brazil. Chem. Geol. 84, 375–376.

Mena, M., Orgeira, M.J., Lagorio, S., 2006. Paleomagnetism, rock-magnetism and geochemical aspects of early Cretaceous basalts of the Paraná Magmatic Province, Misiones, Argentina. Earth Planets Space 58, 1283–1293.

Morey, G.B., Setterholm, D.R., 1997. Rare earth elements in weathering profiles and sediments of Minnesota: implications for provenance studies. J. Sediment. Res. 67, 105–115.

Mugo, R.K., Orians, K.J., 1993. Seagoing method for the determination of chromium(III) and total chromium in sea-water by electron-capture detection gas-chromatography. Anal. Chim. Acta. 271, 1–9.

Nesbitt, H.W., Young, G.M., 1982. Early Proterozoic climates and plate motions inferred from major element chemistry of lutites. Nature 199, 715–717.

Oliveira, M.T.G., Formoso, M.L.L., Trescases, J.J., Meunier, A., 1998. Clay mineral facies and laterization in basalts of the southeastern Parana Basin, Brazil. J. S. Am. Earth Sci. 11, 365–377.

Oze, C., Bird, D.K., Fendorf, S., 2007. Genesis of hexavalent chromium from natural sources in soil and groundwater. Proc. Natl. Acad. Sci. 104, 6544–6549.

Palmer, C.D., Puls, R.W., 1994. Natural attenuation of hexavalent chromium in groundwater and soils, U.S. EPA Ground Water Issue Paper, EPA/540/S-94/505 (U.S. EPA, Office of Researh and Development, Washington, October 1994). U.S. EPA Ground Water Issue Paper, EPA/540/S-94/505 (U.S. EPA, Office of Research and Development,Washington, October 1994).

Pankow, J.F., Leta, D.P., Lin, J.W., Ohl, S.E., Shum, W.P., Janauer, G.E., 1977. Analysis for chromium traces in aquatic ecosystem. 2. Study of Cr(III) and Cr(VI) in Susquehanna River Basin of New York and Pennsylvania. Sci. Total Environ. 7, 17–26.

Patino, L.C., Velbel, M.A., Price, J.R., Wade, J.A., 2003. Trace element mobility during spheroidal weathering of basalts and andesites in Hawaii and Guatemala. Chem. Geol. 202, 343–364.

Pettine, M., Camusso, M., Marinotti, W., 1992. Dissolved and particulate transport of arsenic and chromium in the Po River (Italy). Sci. Total Environ. 119, 253–280.

Piccirillo, E.M., Melfi, A.J., 1988. The Mesozoic Flood Volcanism from the Paraná Basin (Brazil): Petrogenetic and Geophysical Aspects. Universidad de São Paolo, San Pablo,.

Piola, A.R., Matano, R.P., Palma, E.D., Möller Jr., O.O., Campos, E.J.D., 2005. The influence of the Plata river discharge on the western South Atlantic shelf. Geophys. Res. Lett. 32, L016063.

Prohaska, F., 1976. The climate of Argentina, Paraguay and Uruguay. In: Schwertfeger, W. (Ed.), Climates of Central and South America. Elsevier Scientific Publishing Company, Amsterdam.

Richard, F.C., Bourg, A.C.M., 1991. Aqueous geochemistry of chromium: a review. Water Res. 25.

Sander, S., Koschinsky, A., 2000. Onboard-ship redox speciation of chromium in diffuse hydrothermal fluids from the North Fiji Basin. Mar. Chem. 71, 83–102.

Schoenberg, R., Zink, S., Staubwasser, M., von Blanckenburg, F., 2008. The stable Cr isotope inventory of solid Earth reservoirs determined by double spike MC-ICP-MS. Chem. Geol. 249, 294–306.

Schroeder, D.C., Lee, G.F., 1975. Potential transformations of chromium in natural waters. Water Air Soil Pollut. 4, 355–365.

Šillerová, H., Chrastný, V., Čadková, E., Komárek, M., 2014. Isotope fractionation and spectroscopic analysis as an evidence of Cr(VI) reduction during biosorption. Chemosphere 95, 402–407.

Trinquier, A., Birck, J.L., Allegre, C.J., 2008. High-precision analysis of chromium isotopes in terrestrial and meteorite samples by thermal ionization mass spectrometry. J. Anal. At. Spectrom. 23, 1565–1574.

Vera, C.S., Vigliarolo, P.K., Berbery, E.H., 2002. Cold season synoptic-scale waves over subtropical South America. Mon. Weather Rev. 130, 684–699.

Wanner, C., Zink, S., Eggenberger, U., Mäder, U., 2012. Assessing the Cr(VI) reduction efficiency of a permeable reactive barrier using Cr isotope measurements and 2D reactive transport modeling. J. Contam. Hydrol. 131, 54–63.

Zech, M., Zech, R., Morrás, H., Moretti, L., Glaser, B., Zech, W., 1996. Late Quaternary environmental changes in Misiones, subtropical NE Argentina, deduced from multi-proxy geochemical analyses in a palaeosol-sediment sequence. Q. Int. 196, 121–136.

Zink, S., Schoenberg, R., Staubwasser, M., 2010. Isotopic fractionation and reaction kinetics between Cr(III) and Cr(VI) in aqueous media. Geochim. Cosmochim. Acta 74, 5729–5745.